

Sensitivity to axion-like particles with a three-beam stimulated resonant photon collider around the eV mass range

Kensuke Homma^{a,1} Fumiya Ishibashi,¹ Yuri Kirita,¹ and Takumi Hasada¹

¹*Graduate School of Advanced Science and Engineering, Hiroshima University, Kagamiyama, Higashi-Hiroshima 739-8526, Japan*

(Dated: December 27, 2022)

Abstract

We propose a three-beam stimulated resonant photon collider with focused laser fields in order to directly produce an axion-like particle (ALP) with the two beams and to stimulate its decay by the remaining one. The expected sensitivity around the eV mass range has been evaluated. The result shows that the sensitivity can reach the ALP-photon coupling down to $\mathcal{O}(10^{-14})$ GeV⁻¹ with 1 J class short-pulsed lasers.

arXiv:2212.13012v1 [hep-ph] 26 Dec 2022

^a corresponding author

I. INTRODUCTION

CP violation is rather naturally expected from the topological nature of the QCD vacuum, θ -vacuum, which is required, at least, to solve the $U(1)_A$ anomaly. Nevertheless, the θ -value evaluated from the measurement of the neutron dipole moment indicates the CP conserving nature in the QCD sector. This so-called strong CP problem is one of the most important problems yet unresolved in the standard model of particle physics. Peccei and Quinn advocated the introduction of a new global $U(1)_{PQ}$ symmetry [1] in order to dynamically cancel out the finite θ -value expected in the QCD sector with a counter θ -value around which a massive axion appears as a result of the symmetry breaking. If the PQ-symmetry breaking scale is much higher than that of the electroweak scale, the coupling of axion to ordinary matter may be feeble. This invisible axion can thus be a reasonable candidate for dark matter as a byproduct.

In addition to axion, axion-like particle (ALP) not necessarily requiring the linear relation between mass and coupling such as in the QCD axion scenario [2], is also important in the context of inflation as well as dark matter in the universe. Among many possible ALPs, the *miracle* model [3] which unifies inflaton and dark matter within a single ALP attracts laser-based experimental searches, because the preferred ranges of the ALP mass (m_a) and its coupling to photons (g/M) are $0.01 < m_a < 1$ and $g/M \sim 10^{-11} \text{ GeV}^{-1}$, respectively, based on the viable parameter space consistent with the CMB observation.

So far we have advocated a method to directly produce axion-like particles and simultaneously stimulate their decays by combining two-color laser fields in collinearly focused geometry [4]. This quasi-parallel photon-photon collision system has been dedicated to sub-eV axion mass window and the searches have been actually performed [5–9]. Given the axion mass window above eV and a typical laser photon energy of $\sim 1 \text{ eV}$, stimulated photon-photon collisions with different collision geometry has a potential to be sensitive to a higher mass window. In addition to the well-known axion helio- and halo-scopes, the proposed method can cooperatively provide unique test grounds totally independent of any of implicit theoretical assumptions on the axion flux in the Sun as well as in the universe. Therefore, if any of the helio- or halo-scopes detects a hint on an ALP, this method can unveil the nature of the ALP via the direct production and its stimulated decay in laboratory-based experiments by tuning the sensitive mass range to that specific mass window. In this sense

it is indispensable for us to prepare the independent method for expanding its sensitive mass window as wide as possible.

In this paper we propose a three-beam laser collider and discuss its expected sensitivity to an unexplored domain for the *miracle* model as well as the benchmark models of the QCD axion based on a realistic set of beam parameters available at world-wide high-intensity laser systems.

II. FORMULATION DEDICATED FOR A STIMULATED THREE BEAM COLLIDER

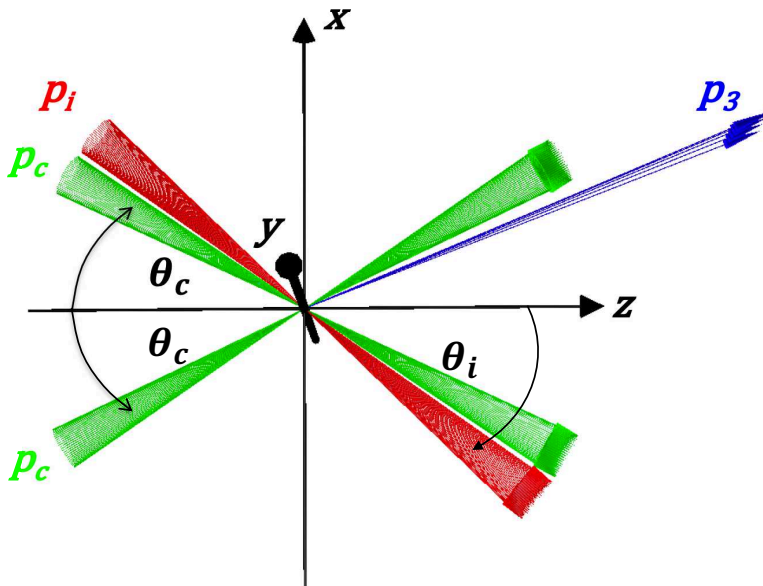


FIG. 1: Schematic view of a three-beam stimulated photon collider.

We focus on the following effective Lagrangian describing the interaction of an ALP as a pseudoscalar field ϕ_a with two photons

$$-\mathcal{L} = \frac{1}{4} \frac{g}{M} F_{\mu\nu} \tilde{F}^{\mu\nu} \phi_a. \quad (1)$$

As illustrated in Fig.1, in the averaged or approximated sense, we consider a coplanar scattering with four-momenta $p_i (i = 1 - 4)$

$$\langle p_c(p_1) \rangle + \langle p_c(p_2) \rangle \rightarrow p_3 + \langle p_i(p_4) \rangle, \quad (2)$$

where two focused laser beams, $\langle p_c \rangle$, create an ALP with a symmetric incident angle θ_c and the produced ALP simultaneously decays into two photons due to an inducing laser beam in the background, $\langle p_i \rangle$, incident with a different angle θ_i . As a result of the stimulated decay, emission of a signal photon p_3 , is induced. $\langle \rangle$ symbols reflect the fact that all three beams contain energy and momentum (angle) spreads at around the focal point. The energy uncertainty is caused by Fourier limited short pulsed lasers such as femtosecond lasers with the optical frequency, while the momentum uncertainty, fluctuations on angle of incidence, is unavoidable due to focused fields. Thus p_1 , p_2 and p_4 must be stochastically selected from individual beams, while p_3 is generated as a result of energy-momentum conservation via $p_1 + p_2 \rightarrow p_3 + p_4$.

We then assume a search for ALPs by scanning θ_c , equal incident angles of the two creation beam axes, to look for an enhancement of the interaction rate when the resonant condition

$$m_a = E_{cms} = 2\omega_c \sin \theta_c \quad (3)$$

is satisfied, where m_a is the ALP mass, ω_c is the central value of single photon energies in the incident creation laser beams and E_{cms} is center-of-mass system (cms) collision energy between two incident photons. Because individual incident photons fluctuate around the average beam energy ω_c and also around the average incident angle θ_c , this resonance condition has to be evaluated via weighted integral (averaging) over proper fluctuation distributions as we discuss below. In the following subsections we thus review necessary formulae to numerically evaluate the interaction rate by taking generic collision geometry with asymmetric incident energies and asymmetric incident angles into account. This asymmetric treatment is essentially required, because unless we implement the degrees of the spreads at fixed θ_c and ω_c depending on experimental parameters, we cannot determine reasonable discretized steps for the scanning over the ALP mass range of interest.

In our previous work [10] we introduced a theoretical interface allowing the asymmetric treatment in the case where a single focused beam is used for creation of an ALP resonance state and the other focused beam sharing the same optical axis as the creation beam is co-moving for inducing the decay. However, if the sensitive mass range must be increased, we have to introduce two separated incident beams for the creation part. Thus, a modified geometrical treatment for the three separated beams must be reconsidered. In [10] we provided formulae only for the case of the scalar field exchange. In order to discuss ALPs,

we have further extended the formulae to the pseudoscalar exchange case with the proper treatment of polarizations affecting the vertex factors [11]. In the following subsections we will provide necessary formulae developed in [10] and [11] with necessary modifications for the purpose of this paper.

A. Expression for signal yield in stimulated resonant scattering

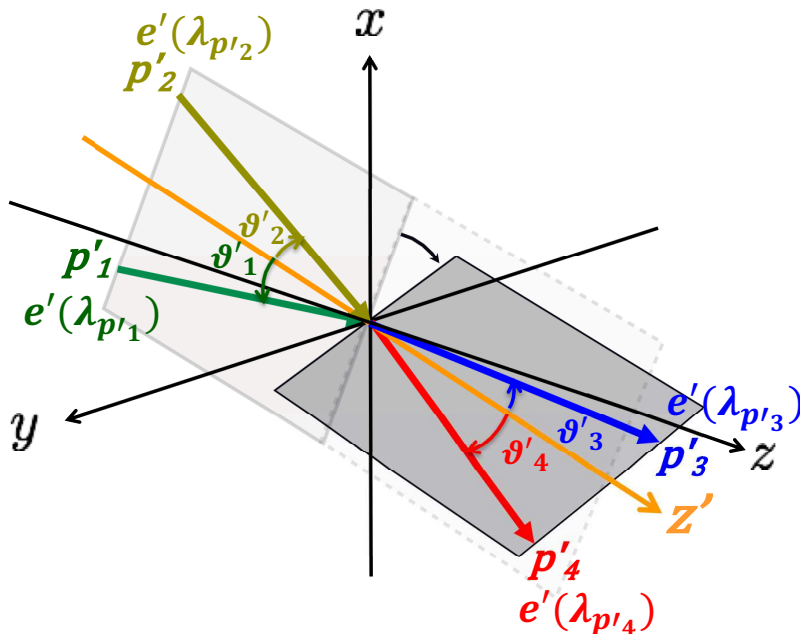


FIG. 2: Relation between theoretical coordinates with the primed symbol and laboratory coordinates to which laser beams are physically mapped. The z' -axis is theoretically obtainable so that stochastically selected two incident photons satisfying the resonance condition have zero pair transverse momentum (p_T) with respect to z' . The Lorentz invariant scattering amplitude is calculated on the primed coordinates where rotation symmetries of the initial and final state reaction planes around z' are maintained. Definitions of four-momentum vectors p'_i and four-polarization vectors $e'(\lambda_{p'_i})$ with polarization states $\lambda_{p'_i}$ for the initial state ($i = 1, 2$) and final state ($i = 3, 4$) plane waves are given. This figure is extracted from [11].

Figure 2 explains the relation between theoretical coordinates with the primed symbol and laboratory coordinates to which laser beams are physically mapped. The z' -axis is theoretically obtainable so that stochastically selected two incident photons satisfying the

resonance condition have zero pair transverse momentum (p_T) with respect to z' . The Lorentz invariant scattering amplitude is calculated on the primed coordinates where rotation symmetries of the initial and final state reaction planes around z' are maintained. Definitions of four-momentum vectors p'_i and four-polarization vectors $e'(\lambda_{p'_i})$ with polarization states $\lambda_{p'_i}$ for the initial-state ($i = 1, 2$) and final-state ($i = 3, 4$) plane waves are given. The conversion between the two coordinates is possible via a simple rotation \mathcal{R} as explained below. In the following, unless confusion is expected, the prime symbol associated with the momentum vectors will be omitted.

We start by reviewing a spontaneous yield of the signal p_3 , \mathcal{Y} , in the scattering process $p_1 + p_2 \rightarrow p_3 + p_4$ only with two incident photon beams having densities ρ_1 and ρ_2 . The concept of *cross section* is useful for fixed p_1 and p_2 beams. In a situation where p_1 and p_2 largely fluctuate within beams, however, its convenience is lost. Thus we apply the following factorization of *volume-wise interaction rate* $\bar{\Sigma}$ [12] instead of *cross section* with units of length L and time s in []

$$\begin{aligned} \mathcal{Y} &= N_1 N_2 \left(\int dt d\mathbf{r} \rho_1(\mathbf{r}, t) \rho_2(\mathbf{r}, t) \right) \times & (4) \\ &\left(\int dQ W(Q) \frac{c}{2\omega_1 2\omega_2} |\mathcal{M}_s(Q')|^2 dL'_{ips} \right) \\ &\equiv N_1 N_2 \mathcal{D} [s/L^3] \bar{\Sigma} [L^3/s] & (5) \end{aligned}$$

where the probability density of cms-energy, $W(Q)$, is multiplied for averaging over the possible range. $W(Q)$ is a function of the combinations of photon energies(ω_α), polar(Θ_α) and azimuthal(Φ_α) angles in laboratory coordinates, denoted as

$$Q \equiv \{\omega_\alpha, \Theta_\alpha, \Phi_\alpha\} \quad \text{and} \quad dQ \equiv \Pi_\alpha d\omega_\alpha d\Theta_\alpha d\Phi_\alpha \quad (6)$$

for the incident beams $\alpha = 1, 2$. The integral with the weight of $W(Q)$ implements the resonance enhancement by including the off-shell part as well as the pole in the s-channel amplitude including the Breit-Wigner resonance function [10, 11].

As illustrated in Fig.2, $Q' \equiv \{\omega_\alpha, \vartheta_\alpha, \phi_\alpha\}$ are kinematical parameters in a rotated coordinates Q' constructed from a pair of two incident wave vectors so that the transverse momentum of the pair with respect to a z' -axis becomes zero. The primed coordinates are convenient because the axial symmetry around the z' -axis allows simpler calculations for the following solid angle integral. The conversions from Q to Q' are thus expressed as rotation matrices on polar and azimuthal angles: $\vartheta_\alpha \equiv \mathcal{R}_{\vartheta_\alpha}(Q)$ and $\phi_\alpha \equiv \mathcal{R}_{\phi_\alpha}(Q)$.

By adding an inducing beam with the central four-momentum p_4 having normalized density ρ_4 with the average number of photons N_4 , we extend the *spontaneous* yield to the *induced* yield, \mathcal{Y}_{c+i} , with the following extended set of kinematical parameters,

$$Q_I \equiv \{Q, \omega_4, \Theta_4, \Phi_4\} \quad \text{and} \quad dQ_I \equiv dQ d\omega_4 d\Theta_4 d\Phi_4. \quad (7)$$

as follows

$$\begin{aligned} \mathcal{Y}_{c+i} &= N_1 N_2 N_4 \left(\int dt d\mathbf{r} \rho_1(\mathbf{r}, t) \rho_2(\mathbf{r}, t) \rho_4(\mathbf{r}, t) V_4 \right) \times \\ &\quad \left(\int dQ_I W(Q_I) \frac{c}{2\omega_1 2\omega_2} |\mathcal{M}_s(Q')|^2 dL'_{ips} \right) \\ &\equiv N_1 N_2 N_4 \mathcal{D}_{three} [s/L^3] \bar{\Sigma}_I [L^3/s], \end{aligned} \quad (8)$$

where the factor $\rho_4(\mathbf{r}, t)V_4$ is a probability corresponding to a degree of spacetime overlap of the p_1 and p_2 beams with the inducing beam p_4 for a given volume of the p_4 beam, V_4 . dL'_{ips} describes an inducible phase space in which the solid angles of p_3 balance solid angles of p_4 via energy-momentum conservation within the distribution of the given inducing beam after conversion from p_4 in the primed coordinate system to the corresponding laboratory coordinate where laser beams are physically mapped. With Gaussian distributions G , $W(Q_I)$ is explicitly defined as

$$W(Q_I) \equiv \Pi_\beta G_E(\omega_\beta) G_p(\Theta_\beta, \Phi_\beta) \quad (9)$$

over $\beta = 1, 2, 4$, where G_E reflecting an energy spread via Fourier transform limited duration of a short pulse and G_p in the momentum space, equivalently the polar angle distribution, are introduced based on the properties of a focused coherent electromagnetic field with an axial symmetric nature for an azimuthal angle Φ around the optical axis of a focused beam, as we discuss below.

1. Evaluation of spacetime overlapping factor \mathcal{D}_{three} with three beams

The factor \mathcal{D}_{three} in Eq.(8) expresses a spatiotemporal overlapping factor of the focused creation beams (subscript $c1$ and $c2$) with the focused inducing beam (subscript i) in laboratory coordinates. The following photon number densities $\rho_{k=c1,c2,i}$ deduced from the electromagnetic field amplitudes based on the Gaussian beam parameterization [13] corre-

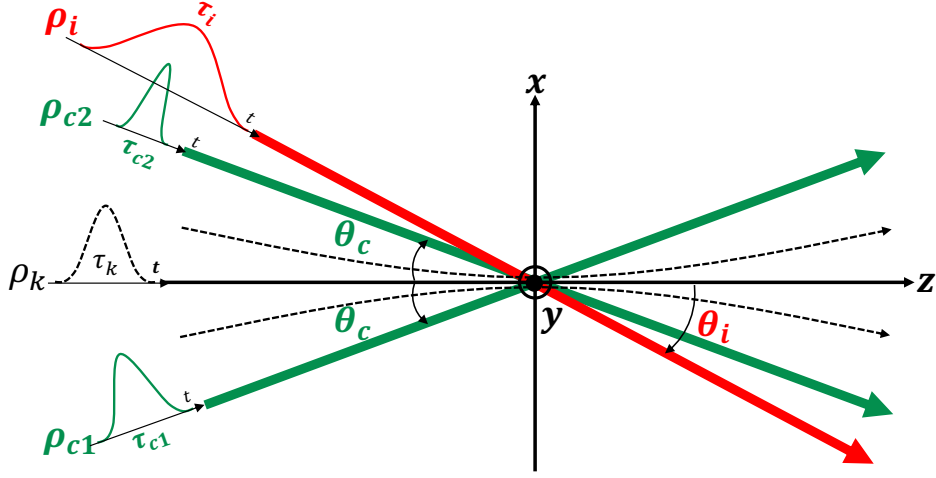


FIG. 3: Collision geometry between three short pulsed laser beams to define the spacetime overlapping factor \mathcal{D}_{three}

sponding to the black pulse in Fig.3 are integrated over spacetime (t, \mathbf{r}) :

$$\rho_k(t, \mathbf{r}) = \left(\frac{2}{\pi}\right)^{\frac{3}{2}} \frac{1}{w_k^2(ct) c\tau_k} \times \exp\left(-2\frac{x^2 + y^2}{w_k^2(ct)}\right) \exp\left(-2\left(\frac{z - ct}{c\tau_k}\right)^2\right), \quad (10)$$

where w_k are the beam radii as a function of time t whose origin is set at the moment when all the pulses reach the focal point, and τ_k are the time durations of the pulsed laser beams with the speed of light c and the volume for the inducing beam V_i is defined as

$$V_i = (\pi/2)^{3/2} w_{i0}^2 c\tau_i, \quad (11)$$

where w_{i0} is the beam waist (minimum radius) of the inducing beam. As a conservative evaluation, the integrated range for the overlapping factor is limited in the Rayleigh length

$$z_{iR} = \frac{\pi w_{i0}^2}{\lambda_i} \quad (12)$$

with the wavelength of the inducing beam λ_i only around the focal point where the induced scattering probability is maximized.

Figure 3 illustrates spacetime pulse functions propagating along individual optical axes of the three beams which are defined by rotating coordinates in Eq.(10) around y -axis. ρ_{c1} ,

ρ_{c2} and ρ_i are defined with the rotation angles: θ_c , $-\theta_c$ and $-\theta_i$, respectively. That is, we assume symmetric incident angles between the two creation laser beams and supply the inducing laser so that photon four-momenta satisfy energy-momentum conservation with respect to a fixed central value for signal photon four-momenta.

The overlapping factor with units of $[s/L^3]$ can be analytically integrated over spatial coordinates and is eventually obtained by numerically integrating over time from $-z_{iR}/c$ to 0 as follows:

$$D_{three} [s/L^3] = \left(\frac{1}{\pi}\right)^{\frac{3}{2}} 2^3 w_{i0}^2 \int_{-\frac{z_{iR}}{c}}^0 dt \frac{1}{w_c^3 w_i c^2 \tau_{c1} \tau_{c2}} \sqrt{\frac{1}{2(2w_i^2 + w_c^2)}} \sqrt{\frac{J}{HS}} \exp\left[\frac{T^2}{4S} - R\right] \exp\left[-2\frac{\tau_{c2}^2 \tau_i^2 + \tau_{c1}^2 \tau_i^2 + \tau_{c1}^2 \tau_{c2}^2 t^2}{\tau_{c1}^2 \tau_{c2}^2 \tau_i^2}\right]. \quad (13)$$

The individual variables in Eq.(13) are summarized as follows, where we use abbreviations $\mathbf{C}_k = \cos \theta_k$ and $\mathbf{S}_k = \sin \theta_k$ for $k = c1, c2, i$ and we assume $\mathbf{C}_c \equiv \mathbf{C}_{c1} = \mathbf{C}_{c2}$, $\mathbf{S}_c \equiv \mathbf{S}_{c1} = \mathbf{S}_{c2}$, $w_c \equiv w_{c1} = w_{c2}$, $d_c \equiv d_{c1} = d_{c2}$ and $f_c \equiv f_{c1} = f_{c2}$, because two creation beams are incident with a symmetric angle and focused with equal beam diameters and focal lengths.

$$\begin{aligned} J [L^6 \cdot s^4] &= w_c^2 w_i^2 c^2 \tau_{c1}^2 \tau_{c2}^2 \tau_i^2, & H [L^4 \cdot s^4] &= 2(2CC_c^2 + DC_i^2 + ES_c^2 + FS_c^2 + GS_i^2), \\ S [1/L^2] &= \frac{O}{J} - P, & T [1/L] &= -(N + Q), \\ R [1] &= -\frac{4}{HJ} (B_c M - B_i G)^2. \end{aligned} \quad (14)$$

The parameters B, C, D, E, F and G are

$$\begin{aligned} B_k [L] &= 2ct\mathbf{S}_k, & C [L^4 \cdot s^4] &= w_i^2 c^2 \tau_{c1}^2 \tau_{c2}^2 \tau_i^2, & D [L^4 \cdot s^4] &= w_c^2 c^2 \tau_{c1}^2 \tau_{c2}^2 \tau_i^2, \\ E [L^4 \cdot s^4] &= w_c^2 w_i^2 \tau_{c2}^2 \tau_i^2, & F [L^4 \cdot s^4] &= w_c^2 w_i^2 \tau_{c1}^2 \tau_i^2, & G [L^4 \cdot s^4] &= w_c^2 w_i^2 \tau_{c1}^2 \tau_{c2}^2. \end{aligned} \quad (15)$$

The parameters M, N, O, P and Q are

$$\begin{aligned} M [L^4 \cdot s^4] &= E - F, & N [1/L] &= 4t \left(\frac{\tau_{c2}^2 \tau_i^2 \mathbf{C}_c + \tau_{c1}^2 \tau_i^2 \mathbf{C}_c + \tau_{c1}^2 \tau_{c2}^2 \mathbf{C}_i}{c\tau_{c1}^2 \tau_{c2}^2 \tau_i^2} \right), \\ O [L^4 \cdot s^4] &= 2(2CS_c^2 + DS_i^2 + EC_c^2 + FC_c^2 + GC_i^2), \\ P [1/L^2] &= \frac{4}{HJ} \{(\mathbf{C}_i \mathbf{S}_i D + \mathbf{C}_c \mathbf{S}_c M)^2 - 2\mathbf{C}_c \mathbf{S}_c \mathbf{C}_i \mathbf{S}_i M G + \mathbf{C}_i^2 \mathbf{S}_i^2 G^2 - 2\mathbf{C}_i^2 \mathbf{S}_i^2 D G\}, \\ Q [1/L] &= \frac{4}{HJ} \{\mathbf{C}_c \mathbf{S}_c M (B_c M + B_i G) - \mathbf{C}_i \mathbf{S}_i (B_c M G - B_i G^2 + D B_i G - D B_c M)\}. \end{aligned} \quad (16)$$

The beam parameters relevant to focused geometry used above are expressed as

$$w_k = w_{k0} \sqrt{1 + \frac{c^2 t^2}{z_{kR}^2}}, \quad w_{k0} = \frac{\lambda_k}{\pi \vartheta_{k0}}, \quad \vartheta_{k0} = \arctan \left(\frac{d_k}{2f_k} \right) \quad (17)$$

with $k = c1, c2, i$.

2. Evaluation of inducible volume-wise interaction rate, $\bar{\Sigma}_I$

Performing the analytical integral for $\bar{\Sigma}_I$ in Eq.(8) is not practical and we are forced to evaluate it with the numerical integral. The expression for $|\mathcal{M}_s(Q')|^2$ in the inducible volume-wise interaction rate is fully explained in [11]. In this paper we focus on how to implement the numerical integral configured for a three-beam collider with focused beams. Figure 4 illustrates the entire flow of the calculation. The left figure depicts the initial state of two scattering photons with incidence of two creation beams (green) and an inducing beam (red), while the right figure indicates the final state photons, that is, the inducing beam photons and signal photons (blue) in the laboratory coordinates by omitting the outgoing two creation beams. The top figure is to remind of the scattering amplitude calculation in the primed coordinates. Probability distribution functions in momentum space G_p as a function of polar angles Θ_i and azimuthal angles Φ_i in the laboratory coordinates and those in energy $G_E(\omega_i)$ for individual photons $i = 1, 2, 4$ are assigned to individual focused beams by denoting the normalized Gaussian distributions as G . The actual steps for the calculations are as follows:

1. Select a finite-size segment of p_1 from given $G_E(\omega_1)G_p(\Theta_1, \Phi_1)$ distributions.
2. Find p_2 which satisfies the following resonance condition

$$m_a = E_{cms} = 2\sqrt{\omega_1\omega_2} \sin \left(\frac{\vartheta_1 + \vartheta_2}{2} \right) \quad (18)$$

with respect to the selected p_1 and to a finite energy segment in $G_E(\omega_2)$ for a given mass parameter m_a . The possible p_2 candidates satisfying the resonance condition form the yellow thin cone around the p_1 -axis reflecting the width of the Breit-Wigner function as shown in the left figure.

3. Form a z' -axis so that the pair transverse momentum, p_T , becomes zero, which is defined as zero- p_T coordinates (primed coordinates) in contrast to the laboratory coordinates to which the three beams are physically mapped. Only a portion of the

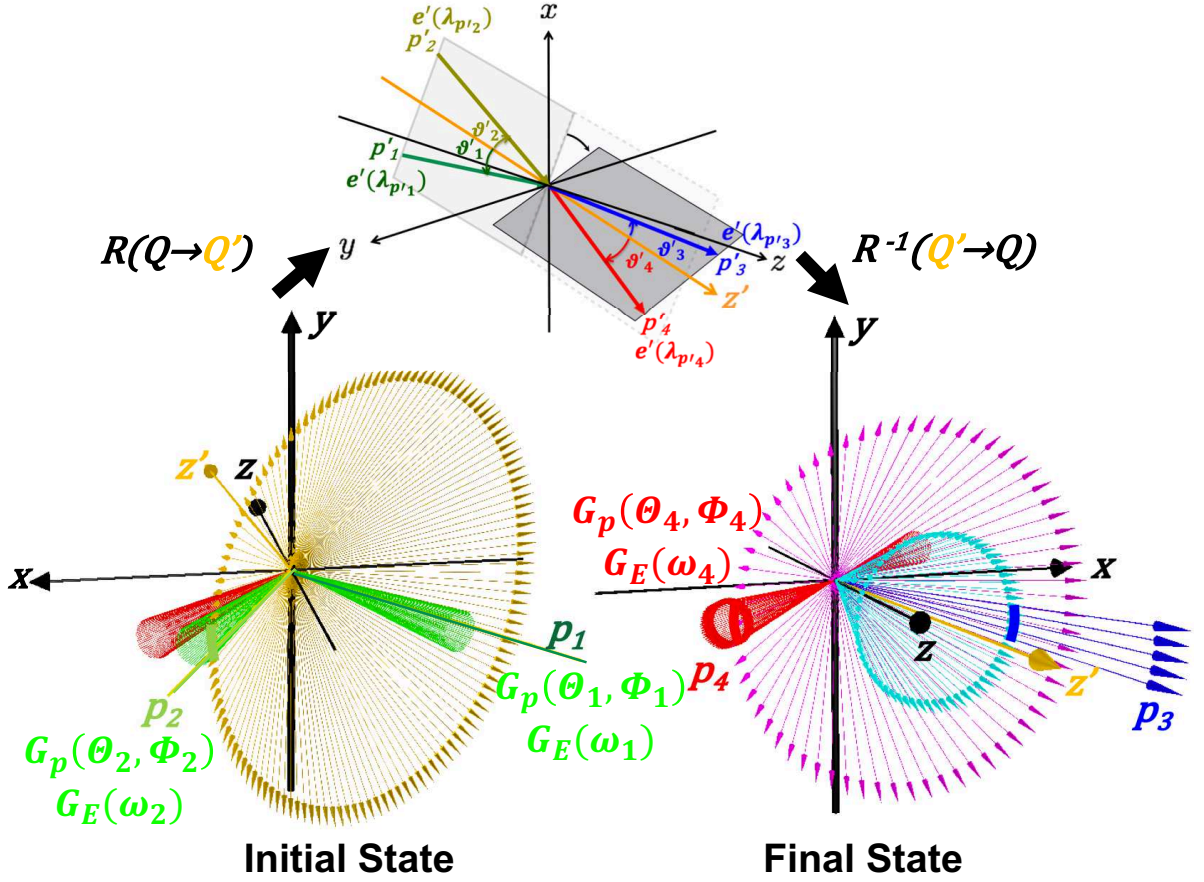


FIG. 4: Flow of the numerical calculation. The left figure depicts the initial state of two scattering photons with incidence of two creation beams (green) and an inducing beam (red), while the right figure indicates the final state photons, that is, the inducing beam photons and signal photons (blue) in the laboratory coordinates by omitting the outgoing two creation beams. The top figure is to remind of the scattering amplitude calculation in the primed coordinates. Probability distribution functions in momentum space G_p as a function of polar angles Θ_i and azimuthal angles Φ_i in the laboratory coordinates and those in energy $G_E(\omega_i)$ for individual photons $i = 1, 2, 4$ are assigned to individual focused beams by denoting the normalized Gaussian distributions as G .

creation beam prepared for p_2 overlapping with the yellow cone can effectively contribute to the resonance production and, hence, the field weight for the pair can be eventually evaluated by properly reflecting $G_E(\omega_1)G_p(\Theta_1, \Phi_1)$ and $G_E(\omega_2)G_p(\Theta_2, \Phi_2)$.

4. Convert the polarization vectors $e_i(\lambda_i)$ as well as the momentum vectors from the laboratory coordinates to the zero- p_T coordinates through the coordinate rotation $\mathcal{R}(Q \rightarrow Q')$.
5. The axial symmetric nature of possible final-state momenta p'_3 and p'_4 around z' is represented by the light-blue and magenta vectors in the right figure. A spontaneous scattering probability with the vertex factors using the primed polarization vectors in the planes containing the four photon wave vectors is calculated in the given zero- p_T coordinates as illustrated in the top figure. By using the axial symmetric nature around z' , the probability can be integrated over possible final state planes containing p'_3 and p'_4 .
6. In order to estimate the inducing effect for given $G_E(\omega_4)G_p(\Theta_4, \Phi_4)$ distributions fixed in the laboratory coordinates, a matching fraction of p_4 is calculated after rotating the primed vectors back to those in the laboratory coordinates from the zero- p_T coordinates via the inverse rotation $\mathcal{R}^{-1}(Q' \rightarrow Q)$. Based on the spread of $G_E(\omega_4)$, the weights along the overlapping belt between the magenta and red vectors in the right figure are taken into account as the enhancement factor for the stimulation of the decay.
7. Due to energy-momentum conservation, p_3 must balance with p_4 . Thus a signal energy spread via $\omega_s \equiv \omega_3 = \omega_1 + \omega_2 - \omega_4$ and also the polar-azimuthal angle spreads by taking the $G_E(\omega_4)G_p(\Theta_4, \Phi_4)$ distributions into account are automatically determined. The volume-wise interaction rate $\bar{\Sigma}_I$ is then integrated over the inducible solid angle of p_3 reflecting all the energy and angular spreads included in the focused three beams.
8. With Eq. (8) the signal yield \mathcal{Y}_{c+i} can be evaluated.

III. EXPECTED SENSITIVITY

We evaluate search sensitivities based on the concept of a three-beam stimulated resonant photon collider (^tSRPC) with variable incident angles for scanning ALP masses around the eV range as illustrated in Fig.1. By assuming high-intensity femtosecond lasers such as Titanium:Sapphire lasers with 1 J pulse energy for simplicity, we consider that two identical

TABLE I: Experimental parameters used to numerically calculate the upper limits on the coupling–mass relations.

Parameter	Value
Central wavelength of creation laser λ_c	800 nm(ω)/400 nm(2ω)/267 nm(3ω)
Relative linewidth of creation laser, $\delta\omega_c / \langle \omega_c \rangle$	10^{-2}
Duration time of creation laser, τ_c	30 fs
Creation laser energy per τ_c , E_c	1 J
Number of creation photons(ω), N_c	4.03×10^{18} photons
Number of creation photons(2ω), N_c	2.01×10^{18} photons
Number of creation photons(3ω), N_c	1.34×10^{18} photons
Beam diameter of creation laser beam, d_c	60 mm
Polarization	linear (P-polarized state)
Central wavelength of inducing laser, λ_i	1300 nm
Relative linewidth of inducing laser, $\delta\omega_i / \langle \omega_i \rangle$	10^{-2}
Duration time of inducing laser beam, τ_i	100 fs
Inducing laser energy per τ_i , E_i	0.1J
Number of inducing photons, N_i	6.54×10^{17} photons
Beam diameter of inducing laser beam, d_i	30 mm
Polarization	circular (left-handed state)
Focal length of off-axis parabolic mirror, $f_c = f_i$	600 mm
Overall detection efficiency, ϵ	1%
Number of shots, N_{shots}	10^5 shots
δN_S	100

creation beams with the central photon energy ω_c and the time duration τ_c are symmetrically incident with the same beam incident angle θ_c and an inducing laser with the central photon energy $\omega_i \equiv u\omega_c$ with $0 < u < 1$ is incident with the corresponding angle which satisfies energy-momentum conservation by requiring a common signal photon energy $(2 - u)\omega_c$ in-

dependent of various incident angle combinations. The central wavelength is around 800 nm and then we assume the ability to produce high harmonic waves from the fundamental wavelength for creation beams and to generate an inducing beam with a non-integer number u based on the optical parametric amplification (OPA) technique in order to discriminate signal waves against the integer number high harmonic waves originating from the creation beams. Since the OPA technique cannot achieve the perfect conversion from the fundamental wavelength, we assume 0.1 J pulse energy and also the elongation of the pulse duration for the inducing beam compared to that in the creation beam. Table I summarizes assumed parameters for two identical creation laser beams and an including laser beams as well as the common focusing and statistical parameters.

Given a set of three-beam laser parameters P in Table I, the number of stimulated signal photons, N_{obs} , is expressed as

$$N_{obs} = \mathcal{Y}_{c+i}(m_a, g/M; P) N_{shot} \epsilon, \quad (19)$$

which is a function of ALP mass m_a and coupling g/M , where N_{shot} the number of laser shots and ϵ the overall efficiency of detecting p_3 . For a set of m_a values with an assumed N_{obs} , a set of coupling g/M can be estimated by numerically solving Eq.(19).

Based on parameters in Table I, Fig.5 shows the reachable sensitivities in the coupling-mass relation for the pseudoscalar field exchange at a 95% confidence level by t SRPC. The red, blue, and magenta solid/dashed curves show the expected upper limits by t SRPC when we assume $\omega_c = 800$ nm (fundamental wavelength ω), 400 nm (second harmonic 2ω) and 267 nm (third harmonic 3ω), respectively. The ALP mass scanning is assumed to be performed with the step of 0.1 eV. Thanks to energy and momentum fluctuations at around the focal point, the same order sensitivities are maintained within the assumed scanning step (the local minima of the parabolic behavior in the coupling correspond to different incident angle setups in Fig.5). For easy viewing, the solid and dashed curves are drawn alternatively. These assumed photon sources are all available within the current technology [14] in terms of the photon wavelength and energy per pulse.

These sensitivity curves are obtained based on the following condition. In this virtual search, the null hypothesis is supposed to be fluctuations on the number of photon-like signals following a Gaussian distribution whose expectation value, μ , is zero for the given total number of collision statistics. The photon-like signals implies a situation where photons-like

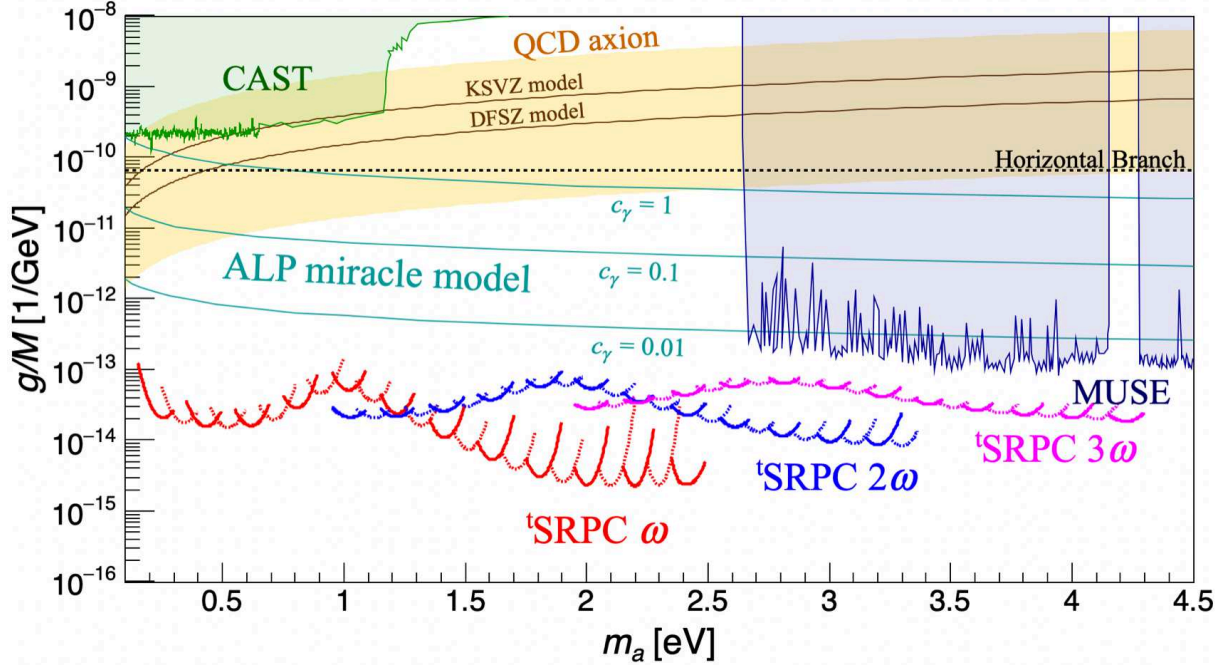


FIG. 5: Expected sensitivities in the coupling-mass relation for the pseudoscalar field exchange at a 95% confidence level by a three-beam stimulated resonant photon collider (t SRPC) with focused short-pulsed lasers based on the beam parameters in Table I.

peaks are counted by a peak finder based on digitized waveform data from a photodevice [8], where electrical fluctuations around the baseline of a waveform cause both positive and negative numbers of photon-like signals. In order to exclude this null hypothesis a confidence level $1 - \alpha$ is introduced as

$$1 - \alpha = \frac{1}{\sqrt{2\pi}\sigma} \int_{\mu-\delta}^{\mu+\delta} e^{-(x-\mu)^2/(2\sigma^2)} dx = \text{erf}\left(\frac{\delta}{\sqrt{2}\sigma}\right), \quad (20)$$

where μ is the expected value of an estimator x following the hypothesis, and σ is one standard deviation. In this search, the estimator x corresponds to the number of signal photons N_S and we assume the detector-acceptance-uncorrected uncertainty δN_S as the one standard deviation σ around the mean value $\mu = 0$. For setting a confidence level of 95%, $2\alpha = 0.05$ with $\delta = 2.24\sigma$ is used, where a one-sided upper limit by excluding above $x + \delta$ [15] is considered. For a set of experimental parameters P in Table I, the upper limits on the coupling-mass relation, m_a vs. g/M , are then estimated by numerically solving the following equation

$$N_{obs} = 2.24\delta N_S = \mathcal{Y}_{c+i}(m_a, g/M; P) N_{shots} \epsilon. \quad (21)$$

The horizontal dotted line shows the upper limit from the Horizontal Branch (HB) observation [16]. The purple area shows bounds by the optical MUSE-faint survey [17]. The green area is excluded by the helioscope experiment CAST [18]. The yellow band shows the QCD axion benchmark models with $0.07 < |E/N - 1.95| < 7$ where KSVZ($E/N = 0$) [19] and DFSZ($E/N = 8/3$) [20] are shown with the brown lines. The cyan lines show predictions from the ALP *miracle* model [3] with its intrinsic model parameters $c_\gamma = 1.0, 0.1, 0.01$, respectively.

IV. CONCLUSION

We have evaluated expected sensitivities to axion-like particles coupling to photons based on the concept of a three-beam stimulated resonant photon collider with focused short-pulse lasers. Within the current high-intensity laser technology reaching the pulse energy 1 J, we found that the searching method can probe ALPs in the eV mass range down to $g/M = \mathcal{O}(10^{-14}) \text{ GeV}^{-1}$. This sensitivity is sufficient to test the unexplored domain motivated by the *miracle* model as well as the benchmark QCD axion models.

ACKNOWLEDGMENTS

K. Homma acknowledges the support of the Collaborative Research Program of the Institute for Chemical Research at Kyoto University (Grant Nos. 2018–83, 2019–72, 2020–85, 2021–88, and 2022–101) and Grants-in-Aid for Scientific Research Nos. 17H02897, 18H04354, 19K21880, and 21H04474 from the Ministry of Education, Culture, Sports, Science and Technology (MEXT) of Japan. Y. Kirita acknowledges support from the JST, the establishment of university fellowships for the creation of science technology innovation, Grant No. JPMJFS2129, and a Grant-in-Aid for JSPS fellows No. 22J13756 from the Ministry of Education, Culture, Sports, Science and Technology (MEXT) of Japan.

[1] R. D. Peccei and H. R. Quinn, Phys. Rev. Lett **38**, 1440 (1977)

- [2] S. Weinberg, Phys. Rev. Lett **40**, 223 (1978); F. Wilczek, Phys. Rev. Lett **40**, 271 (1978); J. E. Kim, Phys. Rev. Lett. **43**, 103 (1979); M. A. Shifman, A. I. Vainshtein and V. I. Zakharov, Nucl. Phys. B **166**, 493 (1980).
- [3] Ryuji Daido et al., "The ALP miracle revisited", Journal of High Energy Physics, 02 (2018) 104, 16th February 2018.
- [4] Y. Fujii and K. Homma, Prog. Theor. Phys **126**, 531 (2011); Prog. Theor. Exp. Phys. 089203 (2014) [erratum].
- [5] K. Homma, T. Hasebe, and K.Kume, Prog. Theor. Exp. Phys. 083C01 (2014).
- [6] T. Hasebe, K. Homma, Y. Nakamiya, K. Matsuura, K. Otani, M. Hashida, S. Inoue, S. Sakabe, Prog. Theo. Exp. Phys. 073C01 (2015).
- [7] A. Nobuhiro, Y. Hirahara, K. Homma, Y. Kirita, T. Ozaki, Y. Nakamiya, M. Hashida, S. Inoue, and S. Sakabe, Prog. Theo. Exp. Phys. 073C01 (2020).
- [8] K. Homma, Y. Kirita, M. Hashida, Y. Hirahara, S. Inoue, F. Ishibashi, Y. Nakamiya, L. Neagu, A. Nobuhiro, T. Ozaki, M. Rosu, S. Sakabe and O. Tesileanu (SAPPHIRES), Journal of High Energy Physics, 12, (2021) 108.
- [9] Y. Kirita, T. Hasada, M. Hashida, Y. Hirahara, K. Homma, S. Inoue, F. Ishibashi, Y. Nakamiya, L. Neagu, A. Nobuhiro, T. Ozaki, M. Rosu, S. Sakabe and O. Tesileanu (SAPPHIRES), Journal of High Energy Physics, 10, (2022) 176.
- [10] Kensuke Homma and Yuri Kirita, Journal of High Energy Physics, 09, (2020) 095.
- [11] Kensuke Homma, Yuri Kirita, Fumiya Ishibashi, Universe 7 (2021) 12, 479.
- [12] J. D. Bjorken and S. D. Drell, *Relativistic Quantum Mechanics*, McGraw-Hill, Inc. (1964); See also Eq.(3.80) in W. Greiner and J. Reinhardt, *Quantum Electrodynamics Second Edition*, Springer (1994).
- [13] Amnon Yariv, *Optical Electronics in Modern Communications* Oxford University Press (1997).
- [14] <https://eli-laser.eu>
- [15] See Eq.(36.56) in J. Beringer *et al.* (Particle Data Group), Phys. Rev. D **86**, 010001 (2012).
- [16] A. Ayala et al., Phys. Rev. Lett. **113**, 19, 191302 (2014).
- [17] Marco Regis, Marco Taoso, Daniel Vaz, Jarle Brinchmann, Sebastiaan L. Zoutendijk, Nicolas F. Bouché, Matthias Steinmetz, Physics Letters B, 814 (2021) 136075.
- [18] V. Anastassopoulos et al. (CAST), Nature Phys. **13**, 584 (2017).

- [19] J. E. Kim, *Phys. Rev. Lett.* 43, 103 (1979); M. Shifman, A. Vainshtein, and V. Zakharov, *Nucl. Phys.* B166, 493 (1980).
- [20] M. Dine, W. Fischler, and M. Srednicki, *Phys. Lett.* 104B, 199 (1981); A. Zhitnitskii, *Sov. J. Nucl. Phys.* 31, 260 (1980).